Holocene right-slip rate determined by cosmogenic and OSL dating on the Anar fault, Central Iran

Kristell Le Dortz, Bertrand Meyer, Michel Sébrier, H. Nazari, Regis Braucher, M. Fattahi, L Benedetti, M. Foroutan, Lionel Siame, D. Bourles, et al.

Geophys. J. Int. (2009) **179,** 700–710 doi: 10.1111/j.1365-246X.2009.04309.x

Holocene right-slip rate determined by cosmogenic and OSL dating on the Anar fault, Central Iran

K. Le Dortz,[1,2] B. Meyer,[1,2] M. Sébrier,[1,2] H. Nazari,[3] R. Braucher,[4] M. Fattahi,[5,6] L. Benedetti,[4] M. Foroutan,[3] L. Siame,[4] D. Bourlès,[4] M. Talebian,[3] M. D. Bateman[5] and M. Ghoraishi[3]

[1] *UPMC Univ Paris* 06, *ISTEP,* UMR 7193, F-75005, *Paris, France. E-mail: kristell.le_dortz@upmc.fr*
[2] *CNRS, ISTEP,* UMR 7193; F-75005, *Paris, France*
[3] *Geological Survey of Iran,Teheran, Iran*
[4] *CEREGE* UMR6635, *Aix-En-provence, France*
[5] *The Institute of geophysics, University of Tehran, Kargar Shomali, Tehran, Iran*
[6] *Sheffield Centre for International Drylands Research, Department of geography, University of Sheffield, Winter Street, Sheffield* S10 2TN, *UK*

Accepted 2009 June 24. Received 2009 June 24; in original form 2008 October 22

SUMMARY

^{10}Be cosmic ray exposure (CRE) and optically stimulated luminescence (OSL) dating of cumulative offset of alluvial fan surfaces have been performed to derive the long-term slip-rate of the Anar fault. At two sites, the comparison between OSL ages obtained within the latest sediments emplaced during the aggradation of the fan and cosmogenic exposure ages of the pebbles abandoned on the surface before its incision and subsequent dextral offset indicates a significant and variable CRE inheritance. Combining offset risers with CRE and OSL dating implies the southern Anar fault slips at a minimum rate of 0.8 mm yr^{-1}, a little faster than formerly estimated by assuming the incision, which created the risers, was coeval with the onset of the Holocene (12 $\pm$ 2 ka). The latest regional incision in the Anar area appears rather coeval with the onset of the early-middle Holocene pluvial episode (6–10.5 ka) evidenced in the neighbouring region of Northern Oman.

Key words: Geomorphology; Seismicity and tectonics; Continental tectonics: strike-slip and transform; Tectonics and landscape evolution; Tectonics and climate interactions.

INTRODUCTION

The Anar fault is a 200-km-long strike-slip fault located within the Central Iran plateau between 30.6°N–55.3°E and 32.3°N–54.8°E, north of the Zagros (Fig. 1). It is the shortest of a series of northerly trending, right-lateral fault system slicing Central and Eastern Iran. The overall fault zone, from the Deshir fault to the west to the Sistan fault zone along the eastern margin of the Lut desert, is 700 km wide (e.g. Walker & Jackson 2004; Meyer *et al.* 2006). The whole system accounts for a NS right-lateral shear that absorbs the differential motion between the widespread Iran collision zone to the west, and the narrow Makran subduction zone to the east. Although the relative contributions of individual fault zones remain unknown, the overall dextral shear amounts to 16 mm yr^{-1} according to GPS measurements and appears to be accounted for mostly by the edges of the Lut (Vernant *et al.* 2004), to the east of the Anar fault. Despite the absence of resolvable GPS deformation for Central Iran over time-periods of 2 yr (Vernant *et al.* 2004) and 6 yr (Masson *et al.* 2007), and despite the lack of seismicity in the vicinity of the Anar fault, there is clear morphological evidence that the Anar fault is active (Meyer & Le Dortz 2007). A slip-rate of 0.5–0.75 mm yr^{-1} has been inferred through a morphoclimatic scenario that assigns offset-risers an age of 12 $\pm$ 2 ka (Meyer & Le Dortz 2007).

We combine here results of offset measurements with ages of geomorphic markers to derive a direct measurement of the rate of slip on the Anar Fault. First, we summarize the regional tectonic setting and the overall morphology of the Anar fault zone. Then, we describe the detailed morphology of two sites recognized by Meyer & Le Dortz (2007) and for which cosmic ray exposure (CRE) and optically stimulated luminescence (OSL) dating of offset-risers allows determination of the slip-rate. Finally, we revisit the slip-rates inferred for other dextral faults slicing Central and Eastern Iran in the light of that now determined for the Anar fault.

GEOLOGICAL SETTING AND OVERALL MORPHOLOGY OF THE ANAR FAULT ZONE

The Anar fault zone is a strike-slip fault involving two distinctive portions that disrupt the morphology and the structure of the Central Iran Plateau (Fig. 1). The northern portion is located within the mountains with several closely spaced splays cutting across the

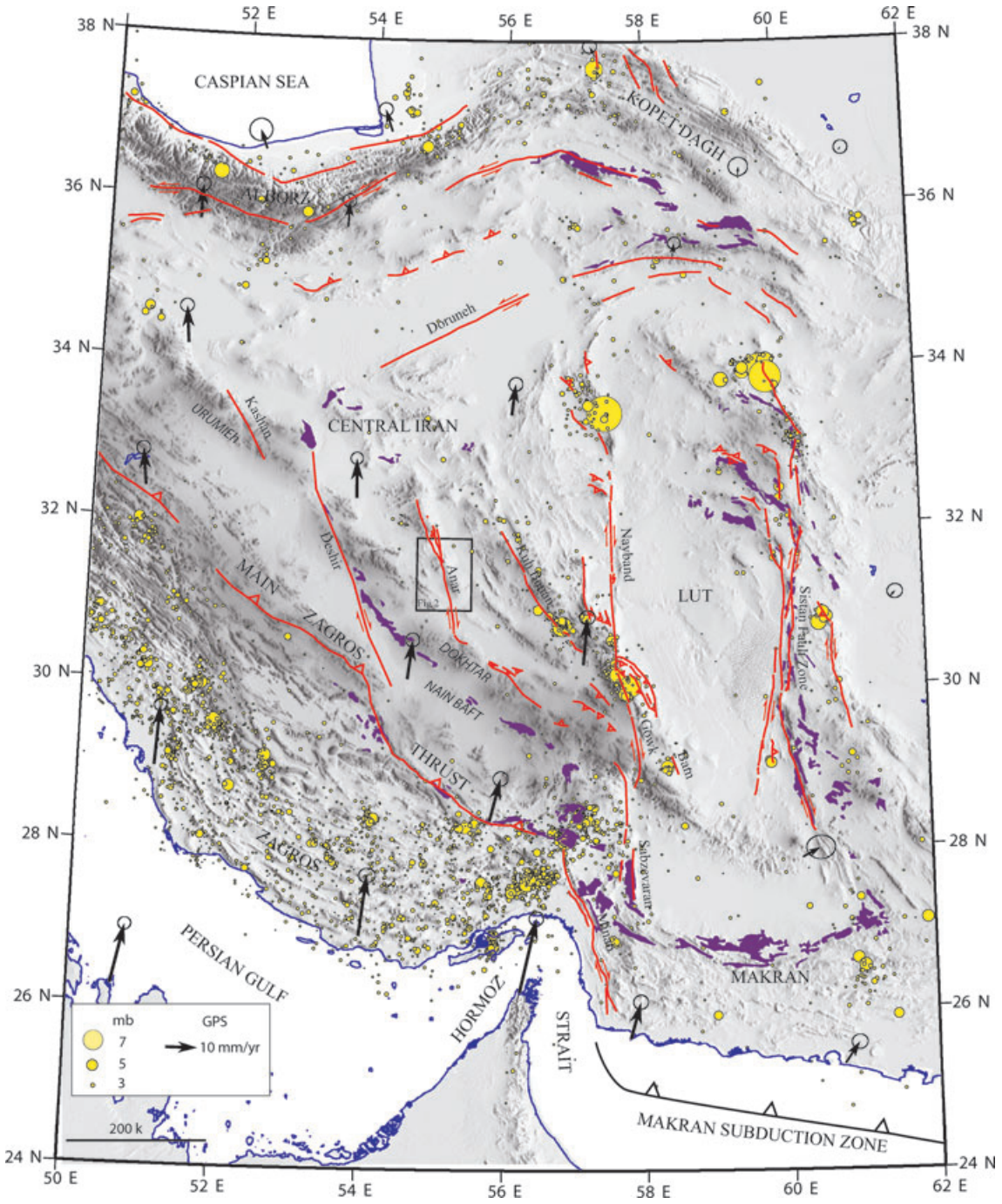

Figure 1. Map of the major active faults of Central and Eastern Iran. The background DEM image is from SRTM data. GPS velocities (black arrows) in Eurasian-fixed reference frame from Vernant *et al.* (2004). The 1973–2007 earthquake distribution (yellow dots) is from NEIC (http://neic.usgs.gov/neis/epic/epic_rect.html). Ophiolite outcrops and sutures are shown as purple patches. The box locates Fig. 2.

relief of the Kuh-e-Kharanaq range (Fig. 2). The splays merge southward extending into a single fault trace. The southern fault strand runs along the Kuh-e-Bafq range over a 20-km-long distance, and cuts right across the western piedmont of the range and across the Anar Salt flat. Further south, the fault bends eastwards, to reactivate a thrust fault to the north of the Urumieh Dokhtar magmatic arc. The total dextral offset is outlined by the displacement on the order of 20–30 km of a Lower Cretaceous sandstone unit (Fig. 2, Walker & Jackson 2004; Meyer & Le Dortz 2007). The ongoing strike-slip tectonics initiated after a widespread Palaeogene shortening stage associated with the emplacement of the Kerman conglomerate. The shortening followed the Late Cretaceous–Early Tertiary closure of the Nain Baft suture and lasted until the final emplacement of the Main Zagros Thrust, probably by the early Neogene. It is nonetheless unlikely that the difference in height between the Kuh-e-Bafq range and its piedmont is entirely inherited from the Palaeogene shortening. Motion on several active thrusts that run across the eastern piedmont of the range might have contributed, even modestly, to the present elevation of the range (Fig. 2). In the case of the neighbouring Gowk strike-slip fault, such thrusts, sub parallel to

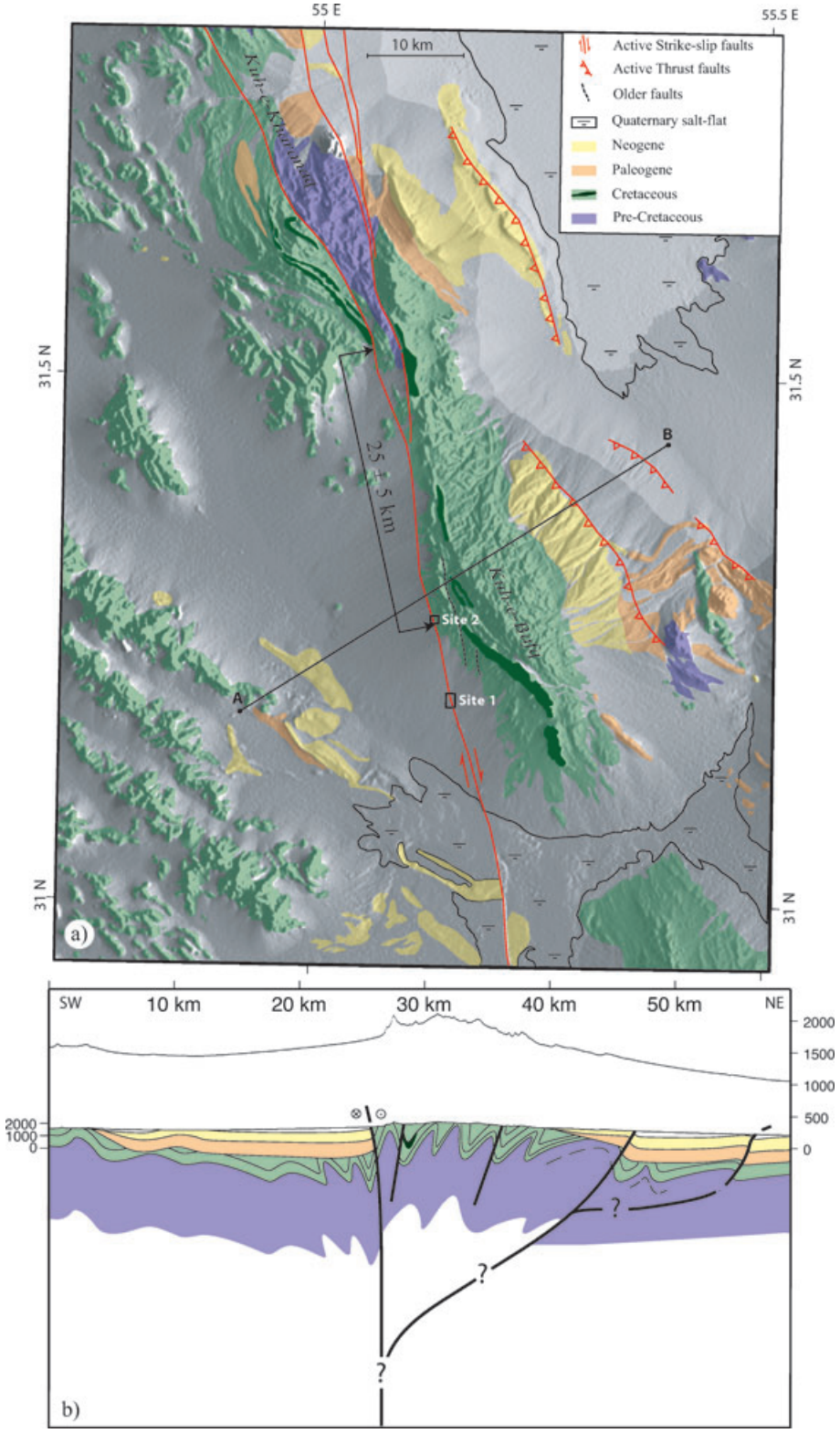

Figure 2. Simplified geological and morphotectonic map of the central part of the Anar fault zone (top panel). Geology is adapted from Yazd (Nabavi 1970) and Anar (Soheili 1981) geological maps and the Landsat and SPOT imagery available. Note the Lower Cretaceous sandstone unit delineating the 25 ± 5 km geological offset. Boxes outline the frames of the Quickbird enlargements in Figs 3 and 4. AB locates the position of the simplified geological cross-section (bottom panel). Topography is also shown with a vertical exaggeration of 5.

the strike-slip, have contributed to the incremental growth of the relief during the 1998 $M_w = 6.6$ Fandoqa strike-slip event (Berberian *et al.* 2001). Similarly to the Gowk fault zone, the Anar strike-slip fault and the faint sub parallel thrust faults, 20 km apart, may root into a single slightly transpressive fault zone at depth (Fig. 2). For the Anar fault zone, however, the lack of documented coeval coseismic motion on the strike-slip and the thrust faults leaves open the possibility of other fault geometries. In any event, the morphological offsets investigated in the next section indicate prevalent dextral motion on a primary strike-slip fault.

OFFSETS MARKERS AND SAMPLING STRATEGY

Morphological evidence of recent motion is clear along the southern strand of the fault where it cuts across coalescent fans fed by intermittent streams flowing west from the 2200-m-high Kuh-e-Bafq mountains. The surface of the fans, further abandoned by the streams as they continued to incise their deposits, stands a few metres above the present streambed that mark the active parts of the fans. At two sites 8 km apart, risers resulting from the incision of ancient streambeds by present ones show dextral offsets. Site 1 locates in the middle of the piedmont where aggradation has been significant and incision has been limited. Numerous small rills and ephemeral streams have incised a few tens of cm into the abandoned fan surface. Longer streams have incised deeper and their wider streambed lie 1–2 m below the surface of the inactive parts of the fans (yellow shading, Fig. 3a). The fault cuts obliquely across the ancient and present streambeds. The scarp, less than a metre high, faces east and disrupts the drainage. Many of the small intermittent rills do not flow through the scarp. They have been isolated from their downstream courses and channelled south eastwards along the scarp. A few larger streams cut through the scarp. The left bank of the largest stream visible in the northern part of the Quickbird extract shows a clear dextral offset. Either in the field or on the imagery, the offset is well constrained and consistent with 8 ± 0.5 m of right-lateral fault motion (Figs 3b and c). Site 2 locates close to the Kuh-e-Bafq Mountains at the faulted contact between recent alluviums and abraded bedrock, where aggradation has been limited and incision has been more significant (Fig. 4a).

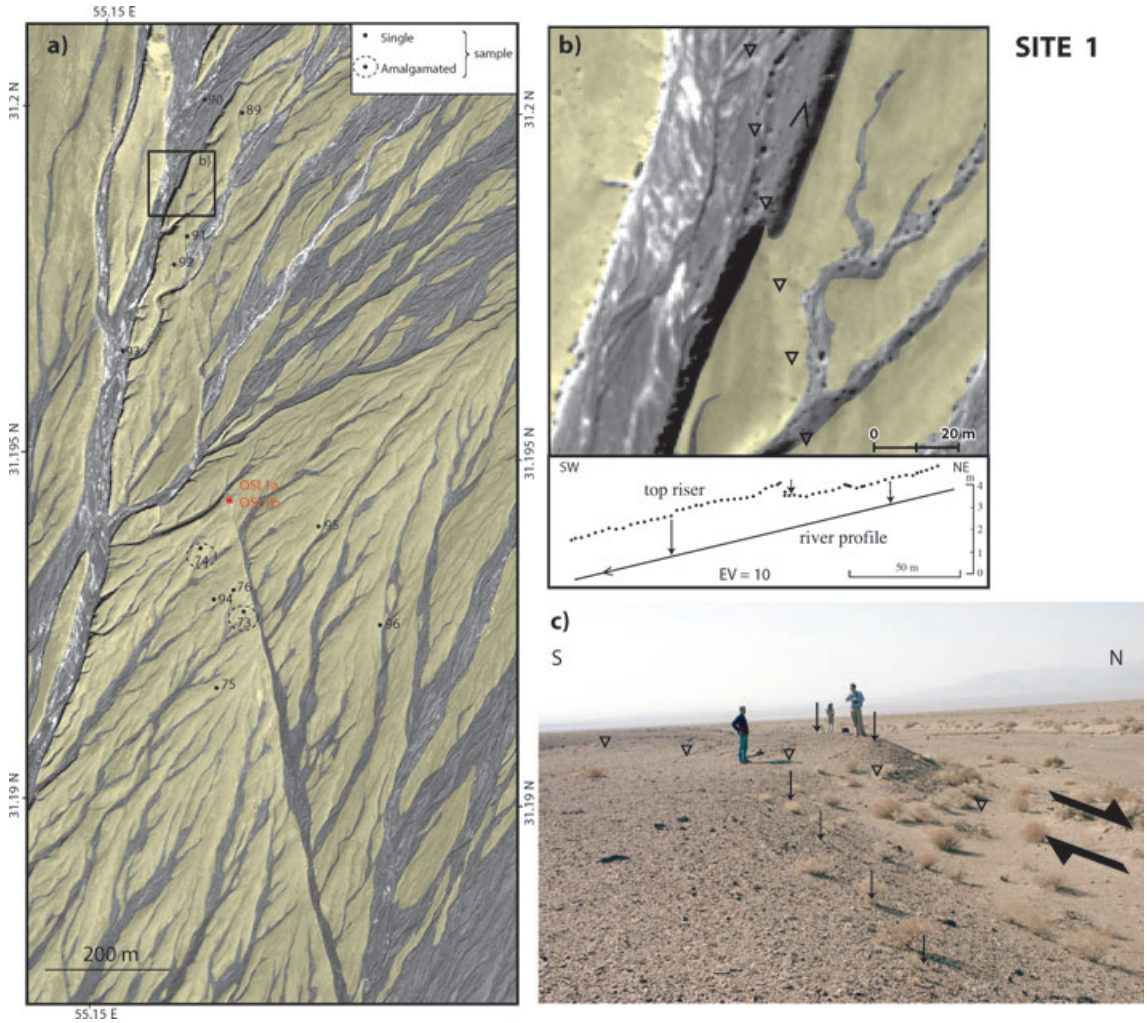

Figure 3. Site 1. (a) Quickbird imagery. The abandoned fan system, yellow shaded, is incised by channels and river streambeds. Numbered dots show position of surface samples collected for cosmogenic dating and dashed circle indicate the sampling area for amalgams. Red square locates position of the subsurface samples collected along the depth-profile in Fig. 5 and the OSL samples taken below the ground surface. (b) Close up on coeval 8 m dextral (top panel) and 0.7 m vertical (bottom panel) offsets of the riser. Open triangles point to the fault trace. Topographic profile (dots for density of the GPS survey) highlights the amount of stream incision up and down scarp. (c) Field photograph of the offset-riser with vertical arrows pointing to the top of the riser.

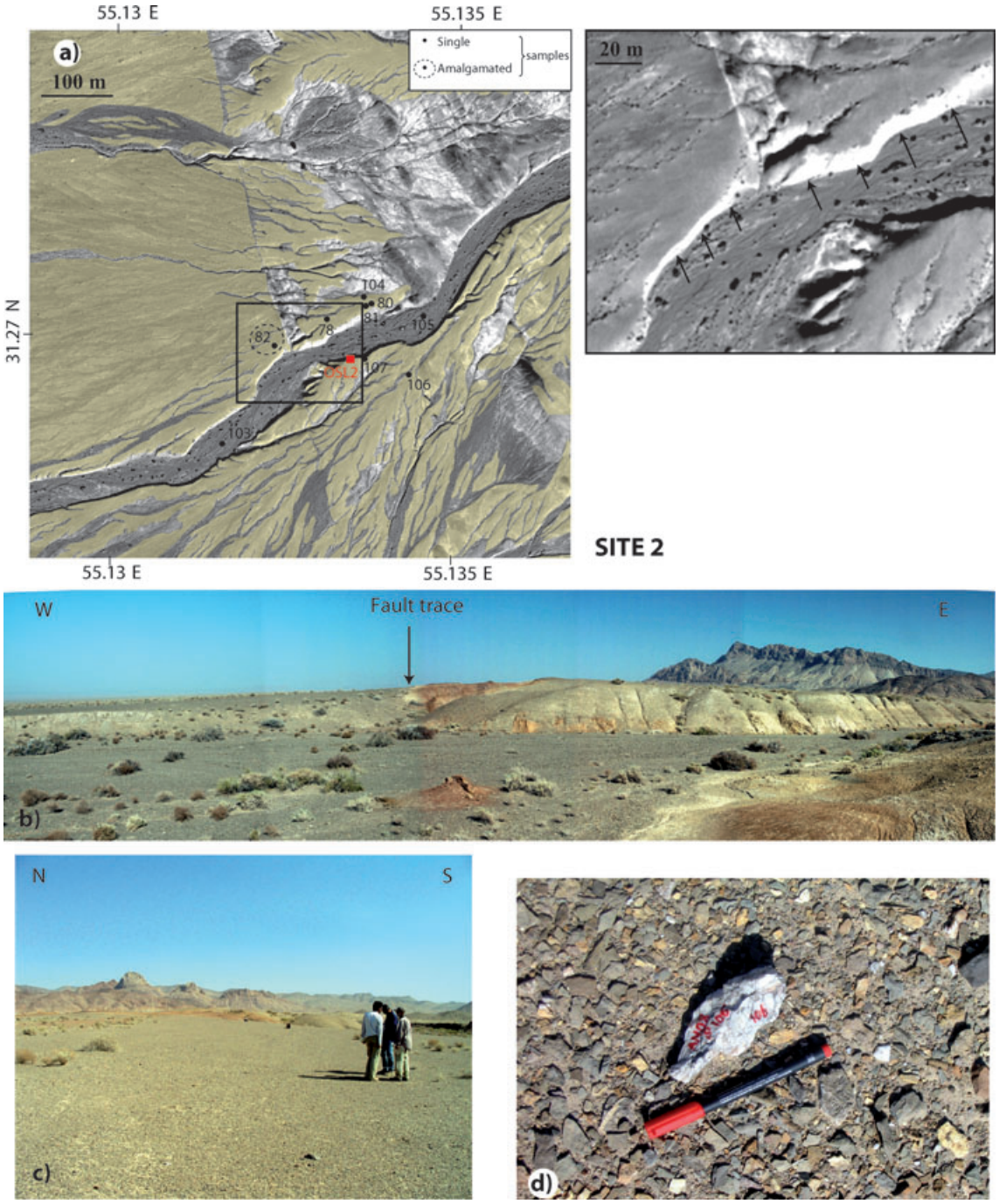

Figure 4. Site 2. (a) Quickbird imagery. Yellow shading denotes the abandoned fan. Numbered dots show position of surface samples collected for cosmogenic dating and dashed circle indicate the sampling area for amalgams. Red square locates the OSL sample collected within the riverbank, 80 cm below the ground surface. Rectangle denotes the close up on the offset riser. Arrows point to the base of the lighted riser. (b) Panoramic view of the right bank of the stream. (c) Overview of the abandoned fan surface, downstream of the fault trace. (d) Close-up of cobbles paving the surface. White cobble is sample AS06S-106 (^{10}Be age of 22 ka).

To the north of the main stream, recent fans crop out west of the fault zone and further to the east where they are unconformable on the abraded bedrock. To the south of the main stream, the fans cover most of the area and the bedrock is no longer discernible. The fault zone cuts entirely across recent sediments and is distinguished by a subdued west-facing scarp. The scarp height is less than a metre and decreases southward. On both sides of the fault, the surface of the fan stands a few metres above the bed of the main intermittent stream. The steep riser cuts provide natural sections of the alluvial deposits typifying the stratigraphy of floodplains and braided channels (Fig. 4b). The sequence starts with coarse conglomerates grading into pebbly-sandy material, and terminates by sandy-silty lenses alternating with conglomeratic layers. East of the fault, the riser is ∼4.5 m high and the erosive contact between the strath deposits and the steeply dipping basement locates close to the base of the riser. West of the fault, the riser is ∼3.5 m high

and cut within the alluvial deposits only. The right-lateral offset measured along the right bank of the stream is 7.5 ± 0.5 m, similar to that at site 1.

At both sites, the offsets have formed since the rivers incised their older floodplains and abandoned the fan surface. Assuming these offsets date from the onset of the Holocene (12 ± 2 ka), Meyer & Le Dortz (2007) hypothesized a slip-rate of 0.5–0.75 mm yr^{-1} that requires further investigation. To constrain the age of incision and abandonment of the fan surface, we sampled quartz-rich sandy layers below the surface for OSL dating and collected quartz-rich pebbles on the surface for measuring the accumulation of cosmogenic nuclides. Both methods are complementary. OSL relies on natural background radioactivity of the material with a small contribution of cosmogenic radiation and measures the time elapsed since the last sunlight exposure of a sediment layer by determining the radiation dose accumulated since its burial and the dose rate due to cosmic radiation. The cosmogenic nuclides, which production decreases rapidly with depth, provide the exposure time resulting from *in situ* interactions between the cosmic rays and the material while exposed at the earth surface.

We collected surface pebbles to estimate their ^{10}Be CRE ages, following a technique pioneered to study erosion-rates (Nishiizumi *et al.* 1984), date alluvial surfaces (e.g. Bierman *et al.* 1995; Anderson *et al.* 1996; Repka *et al.* 1997), and helpful to estimate fault-slip rates (e.g. Ritz *et al.* 1995; Siame *et al.* 1997; Brown *et al.* 1998; Van der Woerd *et al.* 1998). At both sites, the surface of the fans forms a loose desert pavement of varnished clasts separated by a sandy-silty matrix. The clasts are made of locally derived shales, sandstone and conglomerates of the Kuh-e-Bafq Lower Cretaceous formations. The clasts reach in diameter up to tens of centimetres. A few are well rounded, many are angular, and some fragments result from cryoclastic weathering of cobbles and boulders. Very few boulders are unevenly distributed on the abandoned fan surface. We have collected quartz samples from single surface pebbles mainly. In a few cases, small pebbles were amalgamated. For one sample (AS06S-76), we extracted the pebbles from the exposed side of a big boulder of conglomerate. We collected 20 samples on the abandoned fan surface, seven amalgamated samples at increasing depth in a pit dug into the surface and four samples in the present streambeds (Figs 3a and 4a). For the depth profile, each sample corresponds to the amalgamation of ten centimetre-sized clasts, at least.

DATING RESULTS AND DISCUSSIONS

To determine the exposure age of the surface, we measured the concentration of *in situ* produced ^{10}Be that accumulated in the collected

Table 1. The ^{10}Be nuclide concentrations and modelled age for surface and depth-profile samples along the Anar fault.

Sample	Sample description	Latitude (°N)	Longitude (°E)	Altitude (m)	Stone scaling factor	Measured ^{10}Be (10^5 at/g SiO_2)	^{10}Be model age (ka)
Site 1							
AS06S-73	Amalgam-pluricentimetric fragment	31.19474	55.15243	1574	2.73	7.86 ± 0.18	64.85 ± 4.15
AS06S-74	Amalgam-pluricentimetric fragment	31.19404	55.15357	1562	2.71	3.93 ± 0.12	32.11 ± 2.19
AS06S-75	3 fragments of the same gelyfracted pebble	31.19263	55.15304	1571	2.73	2.20 ± 0.05	18.00 ± 1.15
AS06S-76	Conglomerate with pebbles of quartz (cm)	31.19405	55.15330	1559	2.71	2.55 ± 0.06	20.99 ± 1.34
AS08S-89	Fragment of a cobble	31.20095	55.15331	1571	2.73	3.53 ± 0.086	28.91 ± 1.87
AS08S-91	Several fragments of the same gelyfracted pebble	31.19915	55.15242	1571	2.73	3.47 ± 0.08	28.41 ± 1.84
AS08S-92	Amalgam-pluricentimetric fragment	31.19874	55.15221	1570	2.73	3.96 ± 0.10	32.50 ± 2.11
AS08S-94	Two fragments of the same gelyfracted pebble	31.19391	55.15297	1570	2.73	5.20 ± 0.12	42.75 ± 2.77
AS08S-95	Pebble (10 cm)	31.19499	55.15471	1570	2.73	2.70 ± 0.067	22.06 ± 1.43
AS08S-96	Pebble (10 cm)	31.19358	55.15577	1570	2.73	3.83 ± 0.10	31.46 ± 2.08
AS08S-90	Pebble (10 cm) in the river bed	31.20113	55.15268	1571	2.73	1.62 ± 0.06	13.22 ± 0.94
AS08S-93	Pebble (10 cm) in the river bed	31.19748	55.15137	1570	2.73	2.25 ± 0.06	18.38 ± 1.20
Site 2							
AS06S-78	Pebble (15 cm)	31.27033	55.13313	1748	3.09	7.36 ± 0.25	53.60 ± 3.71
AS06S-80	Several fragments of the same gelyfracted pebble	31.27052	55.13378	1751	3.10	5.22 ± 0.12	37.82 ± 2.42
AS06S-81	Fragment of a cobble	31.27046	55.13368	1754	3.09	N.M.	–
AS06S-82	Amalgam	31.26986	55.13239	1743	3.08	10.6 ± 0.23	77.81 ± 4.97
AS08S-104	Two fragments of the same gelyfracted pebble	31.27056	55.13367	1746	3.09	4.49 ± 0.12	32.55 ± 2.15
AS08S-106	Pebble (10 cm)	31.26959	55.13435	1750	3.10	2.99 ± 0.08	21.59 ± 1.42
AS08S-107	Pebble (10 cm)	31.26978	55.1337	1751	3.10	4.3 ± 0.017	31.09 ± 2.05
AS08S-103	Fragment of a big pebble in the river bed	31.26868	55.13163	1741	3.08	0.853 ± 0.06	6.16 ± 0.56
AS08S-105	Pebble (15 cm) in the river bed	31.27033	55.13455	1742	3.08	1.72 ± 0.05	12.45 ± 0.84
Profile[a]							
AS08P-97	Amalgam 370 cm below ground surface	31.19526	55.15340	1567	2.72	4.29 ± 0.12	
AS08P-98	Amalgam 270 cm below ground surface	31.19527	55.15341	1567	2.72	3.48 ± 0.09	
AS08P-99	Amalgam 170 cm below ground surface	31.19527	55.15341	1567	2.72	4.21 ± 0.11	
AS08P-100	Amalgam 100 cm below ground surface	31.19527	55.15341	1567	2.72	2.24 ± 0.06	
AS08P-101	Amalgam 70 cm below ground surface	31.19527	55.15341	1567	2.72	5.15 ± 0.14	
AS08P-102	Amalgam 30 cm below ground surface	31.19527	55.15341	1567	2.72	3.8 ± 0.10	
AS08P-108	Amalgam 150 cm below ground surface	31.19527	55.15341	1567	2.72	1.8 ± 0.05	

Notes: Blank sample with a mean ^{10}Be/^{9}Be ratio of 3×10^{-15}, equivalent to 6×10^4 atoms of ^{10}Be, was used to correct the measured isotopes ratios. Propagated analytical uncertainties include error blank, carrier and counting statistics. Zero erosion model ages are calculated for surface samples with propagated analytical uncertainties and corresponding geographic correction factors. N.M. means no measure.

[a]About 10 pebbles with centimetric size were sampled for each amalgam.

quartz-rich samples exposed to cosmic rays. Samples were prepared following chemical procedures adapted from Brown *et al.* (1991). All samples are crushed and sieved before chemical procedures. Extraction method for ^{10}Be consists in isolation and purification of quartz and elimination of atmospheric ^{10}Be. 100 μl of a 3 $\times$ 10^{-3}gg^{-19}Be solution are added to the decontaminated quartz. Beryllium was separated from the spiked solution obtained after its dissolution in HF by anion and cation exchanges and precipitations. The final precipitate is dried, and heated at 900° C to obtain BeO. Measurements were performed at the new French AMS National Facility, ASTER, located at CEREGE in Aix-en-Provence. The presented data were calibrated directly against the National Institute of Standards and Technology standard reference material 4325 by using the values recently determined by Nishiizumi *et al.* (2007) which are a ^{10}Be/^{9}Be ratio of (2.79 $\pm$ 0.03) $\times$ 10^{-11} and a ^{10}Be half-life of (1.36 $\pm$ 0.07)$\times 10^{6}$ yr. A modern ^{10}Be production rate at sea-level and high-latitude of 4.5 $\pm$ 0.3 atomsg^{-1}yr, computed for internal consistency from the data of Stone (2000) according

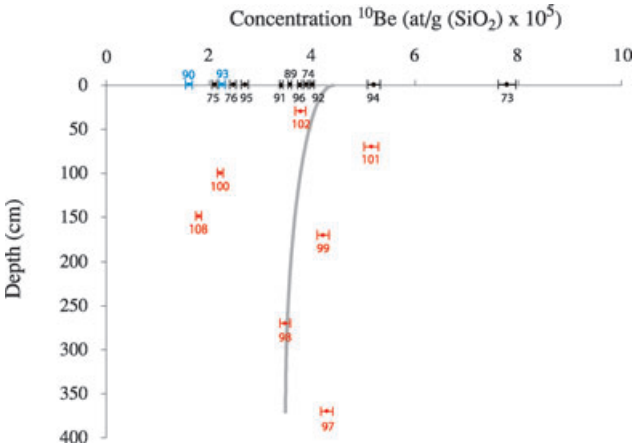

Figure 5. Plot of the measured ^{10}Be concentrations as a function of depth for site 1. Black, red and blue dots are surface, depth-profile and modern stream samples, respectively. The uneven distribution of concentrations for the surface samples and the absence of depth-decreasing concentrations for the subsurface amalgams indicate heterogeneous exposure history and variable inheritance of the fanglomerate material. Forward model of ^{10}Be concentration with depth for a 10 ka surface with no erosion and inheritance of 350.000 atoms per gram is shown for comparison.

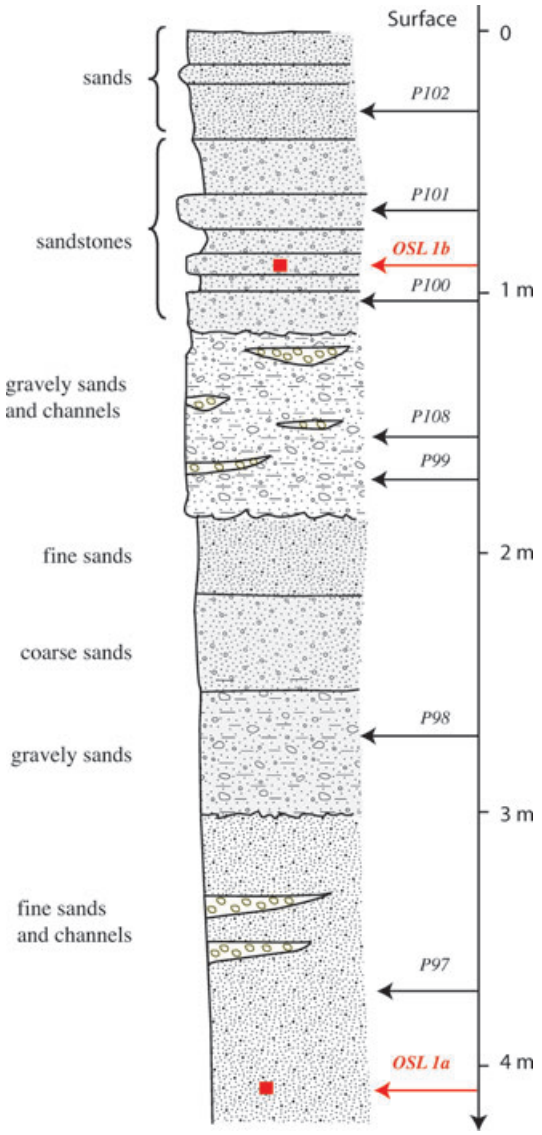

Figure 6. Simplified stratigraphy observed within the pit dug at site 1. Relative position of samples OSL-1a, 1b (red arrows) and CRE subsurface amalgams (blacks arrows) is shown.

Table 2. Equivalent dose (D_e), annual dose rate (D_a) and calculated ages for each sample.

Sample[a]	Sheffield codes	Equivalent dose D_e (Grays)[b]	N[c]	Depth (m)	Water (per cent)	K[d] (per cent)	U[d] (ppm)	Th[d] (ppm)	Annual dose rate D_a (Grays ka^{-1})[e]	Age (ka)[f]
Site 1 (Pit in the surface)										
OSL1a	Shfd08243	12.78 $\pm$ 7.97	21	0.8	2	1.21 $\pm$ 0.01	1.6 $\pm$ 0.05	5.9 $\pm$ 0.1	2.20 $\pm$ 0.05	5.8 $\pm$ 3.6
OSL1b	Shfd08244	23.62 $\pm$ 6.30	10	4.1	0.6	0.93 $\pm$ 0.01	1.16 $\pm$ 0.05	4 $\pm$ 0.1	1.64 $\pm$ 0.05	14.4 $\pm$ 3. 9
Site 2 (Riser)										
OSL2	Shfd08245	22.50 $\pm$ 12.29	16	0.8	1.1	1.06 $\pm$ 0.01	1.33 $\pm$ 0.05	4 $\pm$ 0.1	1.90 $\pm$ 0.05	11.8 $\pm$ 6.5

Note: Ages have been calculated for Quartz grains with size ranging between 90 and 250 μm.
[a]The samples were collected using stainless steel tubes (5 cm $\times$ 25 cm) and both ends were sealed and covered using both aluminium foil and black tape. Quartz was extracted from all samples using standard methods in the Sheffield Centre for International Drylands Research Centre Luminescence Laboratory
[b]Luminescence measured through 7 mm Hoya U-340 filters in a Risø (Model TL/OSL-DA-15) automated TL/OSL system. The equivalent dose (D_e) was obtained using the conventional quartz single aliquot regeneration method (Murray & Wintle 2000). 24 aliquots have been processed for each sample.
[c]N is the number of aliquots out of the 24 not rejected using the quality control parameters and falling within two standard deviations of the mean D_e.
[d]Uranium, thorium and potassium concentrations were measured using inductively coupled plasma mass spectrometer (ICP-MS).
[e]The annual dose (D_a) was estimated from ICP-MS data and the cosmic ray contributions as described in Fattahi *et al.* (2006, 2007).
[f]Errors are 1σ.

to the conclusions of the recently published study on absolute calibration of ^{10}Be AMS standards by Nishiizumi *et al.* (2007), was used. This sea level and high-latitude production rate has then been scaled for the sampling altitudes and latitudes using the scaling factors proposed by Stone (2000) because, using the atmospheric pressure as a function of altitude, they take into account the physical properties of cosmic ray particle propagation in the atmosphere and include an improved account for the muonic component in the total cosmogenic production. Exposure ages were finally calculated with the estimates of the contribution of the nuclear particles given by Braucher *et al.* (2003) and assuming erosion as negligible during the involved time period, they are thus minimum exposure ages (Table 1).

The spread of concentrations, hence CRE calculated ages, is large and testifies for noticeable accumulation of nuclides prior deposition of the pebbles (Table 1). The inheritance is also attested by the significant concentrations measured for the few pebbles (number 90, 93, 103 and 105) collected in the modern streambeds. Depth distribution profiles of cosmogenic nuclide concentrations are sometimes performed to evaluate the inheritance (Anderson *et al.* 1996; Oskin *et al.* 2008). Provided the sediments emplaced in a short period of time (i.e. the same climatic crisis), an exponential decrease of the concentrations helps estimating a homogeneous pre-exposure. The uneven distribution of the concentrations retrieved from a 4 m depth profile within the abandoned fan surface (Fig. 5), together with the scattering of concentrations of the fan surface pebbles as well as of the stream pebbles, dismisses an homogeneous pre-exposure prior to the emplacement of the fan material. The inheritance is variable and may have taken place either during exhumation or transport. The small size of the drainage areas, less than 20 km^2 at both sites, is indicative of a rapid transport before the emplacement of the fans. The scattered surface pebble cosmogenic nuclide concentrations, therefore, indicates the observed inheritance more likely reflects variability of bedrock exhumation rates in the upper catchments rather than a long and complex history of successive burials and exposures during transport by the streams (e.g. Repka *et al.* 1997). The ages on the abandoned alluvial surface range between 18 $\pm$ 1.1 and 77.8 $\pm$ 4.9 kyr, and indicate the whole process of exhumation, transport, and sedimentation occurred during the last glacial period (Fig. 8). By contrast, the few pebbles collected in the present-day streambeds display lower concentrations, hence younger age equivalents. The ages of the river samples range between 6.2 and 18.4 kyr with all but one yielding post-glacial ages. This indicates that the fans likely emplaced until the end of the Last Glacial Stage and have been subsequently incised. Notwithstanding the inheritance, the youngest samples on the surface (samples 75 and 106 with zero erosion model age of 18.0 $\pm$ 1.1 and 21.6 $\pm$ 1.4 kyr, respectively) provide bounds on the abandonment of the surface, the cutting of the risers, and then on the minimum slip-rate. The minimum value for the slip-rate is 0.45 $\pm$ 0.06 mm yr^{-1} at site 1 assuming the age of the 8 $\pm$ 0.5 m offset is at most 18 $\pm$ 1.1 kyr, and 0.34 $\pm$ 0.04 mm yr^{-1} at site 2 assuming the age of the 7.5 $\pm$ 0.5 m offset is at most 21.6 $\pm$ 1.4 kyr.

To refine the former estimate and place independent constraints on the time the incision took place, we aimed at dating the uppermost alluvial layers that were emplaced during the aggradation of the fans. At both sites, we sampled lenses of fine sands at shallow depth below the surface of the fans and applied luminescence dating techniques (Table 2). At site 1, samples OSL1a and OSL1b have been, respectively, collected at 80 cm down and 410 cm down within a pit dug in the middle of the fan surface (Figs 3 and 6). At site 2, sample OSL2 has been directly taken at a depth of 80 cm from the riser of the river (Figs 4 and 7). The OSL age determinations were carried out at the Sheffield Centre for International Dryland research luminescence laboratory (Table 2). Equivalent dose (D_e) values were measured on extracted and cleaned quartz using the Single Aliquot Regeneration (SAR) protocol (e.g. Murray & Wintle 2000). Dose rates received by each samples were based on elemental analysis carried out using ICP at SGS laboratories Ontario, Canada with conversion to annual dose rate using Adamiec & Aitken (1998), Marsh *et al.* (2002) and Aitken (1998) taking into account attenuation factors relating to sediment grain sizes used, density and palaeomoisture. The contribution to dose rates from cosmic sources were calculated using the expression published in Prescott & Hutton (1994). The analytical procedures employed for the Anar samples is similar to that applied to samples from neighbouring Sabzevar and Doruneh areas (Fattahi *et al.* 2006, 2007). Ages were calculated using a mean D_e for each sample (Fig. 9) and ages are presented in Table 2 in years from present (2008) with 1σ errors. For samples OSL1b and OSL2, there were only a few aliquots which met the quality assurance criteria (10 and 16 aliquots, respectively) precluding any meaningful examination of the D_e replicates in terms of establishing whether the samples were partially bleached prior to burial (Fig. 9). In order to counter this, ages for these two samples have been calculated in a very conservative manner using the standard deviation of the weighted (by inverse variance) mean D_e rather than the standard error, which would be normally adopted. As a result, the reported uncertainties on these ages are large (3.6 and 6.5 ka, respectively) and the mean D_e may incorporate an element of over-estimation if partial bleaching has occurred. As Fig. 9 shows, OSL1a has a broad D_e distribution centred around the mean D_e value. For consistency with the other samples and in order to take into account the breath of D_e distribution, the age for this sample has also been calculated conservatively using the standard deviation of the mean D_e. Based on this, the ages for the samples are 14.4 $\pm$ 3.9 kyr (OSL1a), 5.8 $\pm$ 3.6 kyr (OSL1b) and 11.8 $\pm$ 6.5 kyr (OSL2). Whether there has been incomplete resetting of the OSL samples or not, the samples collected 80 cm down at each site (OSL1a at site 1; OSL2 at site 2) provide temporal limits on the cutting of the risers and on the minimum value of the slip-rate. Using the oldest ages, determined by combining the mean age plus the associated 1σ uncertainty, the minimum slip-rate is 0.85 $\pm$ 0.06 mm yr^{-1} at site 1 and 0.41 $\pm$ 0.03 mm yr^{-1} at site 2. This accounts for 8 $\pm$ 0.5 and 7.5 $\pm$ 0.5 m offsets at site 1 and 2, respectively and assumes that site 1 is at most 9.4 kyr old and site 2 at most 18.3 kyr old. The difference of slip-rates between the two sites might be due either to incomplete solar resetting of the older OSL sample or to difference in the sedimentation rate. The constancy of offset riser at both sites rather favours the latter as site 2 is located closer to the mountain and site 1 stands in the middle of the piedmont. The value of 0.85 mm yr^{-1} is therefore a safe lower bound of the slip-rate on the southern segment of the Anar fault.

Finally, it is useful combining OSL and CRE results to discuss the inheritance (Fig. 8a). The risers postdate both the sediments they have incised and the abandonment of the fans. The surface of the fan being younger than the underlying sediments, the oldest possible age of a shallow OSL sample retrieved from these sediments provides a maximum age for the time of surface abandonment, hence an upper bound for the age of surface pebbles without inheritance (9.4 kyr at site 1 and 18.3 kyr at site 2). This confirms there has been a significant accumulation of nuclides before the emplacement of the pebbles and allows calculating the minimum proportion of pre-exposure for CRE age of each surface pebble (arrows, Fig. 8b).

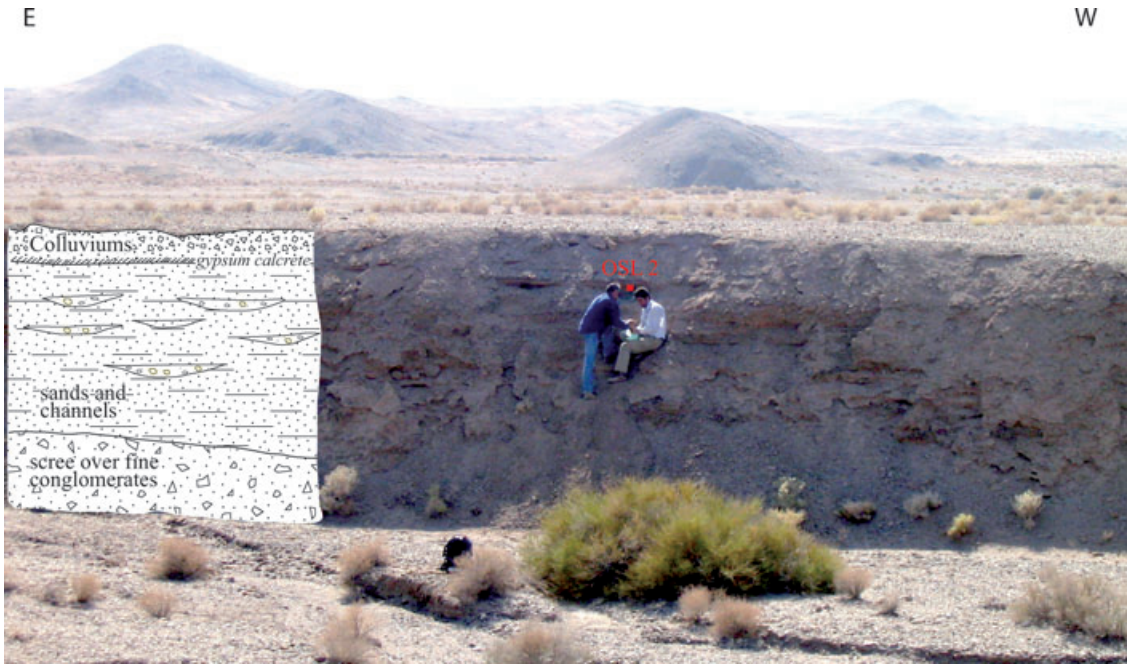

Figure 7. Photograph of the left bank of the river at site 2. Stratigraphy of the riser cut is schematized. The sample OSL-2 has been collected in a sandy layer just above the geologists.

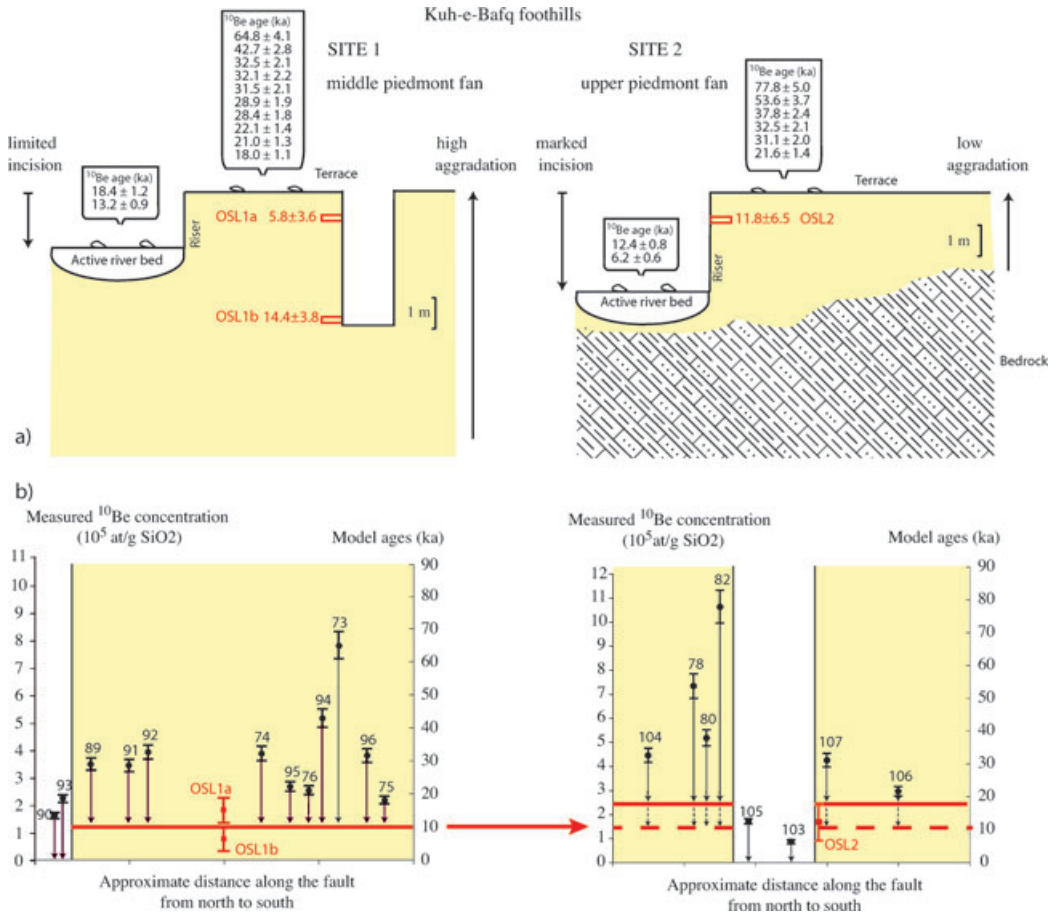

Figure 8. Summary of observations (top) and plot of sample ages in relative position from north to south (bottom) at sites 1 and 2. OSL and CRE surface ages are indicated in red and black, respectively. ^{10}Be concentrations and model ages are indicated by black dots, OSL ages by red squares. Data are tabulated in Tables 1 and 2. Red line is the oldest possible age of the surface strictly compatible at each site with the OSL results. Thick dashed line at site 2 is an extrapolation with the youngest OSL of site 1, see text for discussion. Vertical arrows figure the variable inheritance of individual pebbles.

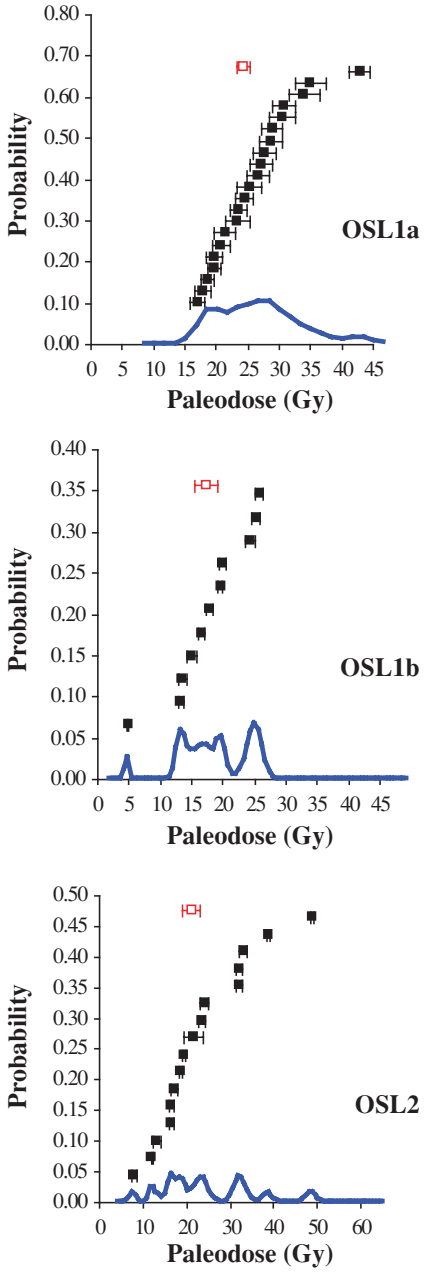

Figure 9. Equivalent dose distribution diagrams from SAR OSL for each of the samples. The equivalent dose distributions are displayed as a combined probability density function (blue curve) with individual aliquot D_e plotted above (filled black squares) and the arithmetic mean of the data (open red square).

CONCLUSION

OSL dating indicates the Anar fans emplaced at the end of the Last Glacial Stage, most probably after the Last Glacial Maximum and during the beginning of the Holocene. The older and scattered CRE ages calculated for the surface and subsurface pebbles indicate that the material eventually incorporated in the fanglomerates has not been uniformly exposed to cosmic rays prior to both fan emplacement and abandonment. The variable CRE inheritance likely originated from a progressive exhumation and alteration of bedrock in the upper catchments of the streams during the Last Glacial Stage. Accounting for the inheritance appears difficult (e.g. Hetzel *et al.* 2006; Oskin *et al.* 2008) and there is no straightforward modelling solution to retrieve the age of the surface. Using CRE ages alone may lead to significant overestimate (50–60 per cent) of the age of a fan surface abandonment, specifically when depth profiles of ^{10}Be concentrations do not help modelling the inheritance.

Considering the Anar region, the incision of the fans is likely younger than the onset of the Holocene (12 ± 2 ka) as proposed by Meyer & Le Dortz (2007). Although relying on a single OSL sample, incision appears younger than 9.4 kyr and allows deriving a safe minimum slip-rate of ∼0.8 mm yr^{-1} on the Anar fault. The incision of the Anar fans appears to correspond to the early-middle Holocene (6–10.5 ka) pluvial period that Burns *et al.* (2001) evidenced by rapid speleothem growth phase in Northern Oman. Burns *et al.* (2001) correlate this pluvial episode and older ones with a significant northward shift of monsoon rainfall during peaks of interglacial periods. It is therefore possible that the regional incision in Central Iran has been driven by the onset of the early-middle Holocene pluvial episode (6–10.5 ka), which has been correlated with lower terraces in Southeastern Iran (Regard *et al.* 2006). This implies that the slip-rates inferred on the strike-slip faults slicing Central and Eastern Iran (Fig. 1) by Meyer & Le Dortz (2007) from the restoration of offset-risers of assumed Holocene age (12 ± 2 kyr) could be underestimated by up to 30 per cent.

ACKNOWLEDGMENTS

This study would have been impossible without financial assistance from INSU-CNRS (PNTS and 3F programs) and from CNES-SPOT Image (ISIS program contracts ISIS0403–622 and ISIS0510–812). KL received a Ministry of Research and Education scholarship granted by the President of University Pierre and Marie Curie. This study benefited from logistic and financial assistance from Geological Survey of Iran. We acknowledge A. Rashidi and B. Oveisi for efficient organization and help during fieldwork. The 10Be measurements were performed at the ASTER AMS national facility (CEREGE, Aix en Provence), which is supported by the INSU/CNRS, the French Ministry of Research and Higher Education, IRD and CEA. We thank L. Leanni, F. Chauvet, M. Arnold and G. Aumaître for their help during chemistry and measurements at CEREGE. MF acknowledges support from the research department of the University of Tehran. We acknowledge reviews by Vincent Regard and Richard Walker. We are grateful to R. Walker for suggesting improvements to the discussion of the OSL results.

REFERENCES

Adamiec, G. & Aitken, M.J., 1998. Dose-rate conversion factors: update, *Ancient TL,* **16,** 37–50.

Aitken, M.J., 1998. *An Introduction to Optical Dating: The Dating of Quaternary Sediments by the Use of Photon-Stimulated Luminescence,* Oxford University Press, Oxford.

Anderson, R.S., Repka, J.L. & Dick, G.S., 1996. Explicit treatment of inheritance in dating depositional surfaces using in situ 10Be and 26Al, *Geology,* **24,** 47–51.

Berberian, M. *et al*., 2001. The 1998 March 14 Fandoqa earthquake Mw6.6 in Kerman, southeast Iran: re-rupture of the 1981 Sirch earthquake fault, triggering of slip on adjacent thrusts, and the active tectonics of the Gowk fault zone, *Geophys. J. Int.,* **146**(2), 371–398.

Bierman, P.R., Gillespie, A.R. & Caffee, M.W., 1995. Cosmogenic ages for earthquake recurrence intervals and debris flow fan deposition, Owens Valley, California, *Science,* **270,** 447–450.

Braucher, R., Brown, E.T., Bourlès, D.L. & Colin, F., 2003. In situ produced 10Be measurements at great depths: implications for production rates by fast muons, *Earth planet. Sci. Lett.,* **211,** 251–258.

Brown, E.T., Edmond, J.M., Raisbeck, G.M., Yiou, F., Kurz, M.D. & Brook, E.J., 1991. Examination of surface exposure ages of Antarctic moraines using in situ produced 10Be and 26Al, *Geochim. Cosmochim. Acta,* **55,** 2699–2703.

Brown, E.T., Bourlès, D.L., Burchfiel, B.C., Deng, Q., Li, J., Molnar, P., Raisbeck, G.M. & You, F., 1998. Estimation of slip rates in the southern Tien Shan using cosmic ray exposure dates of abandoned alluvial fans, *Geol. Soc. Am. Bull.,* **110,** 377–386.

Burns, S.J., Fleitmann, D., Matter, A., Neff, U. & Mangini, A., 2001. Speleothem evidence from Oman for continental pluvial events during ingterglacial periods, *Geology,* **29,** 623–626.

Fattahi, M., Walker, R., Hollingsworth, J., Bahroudi, A., Talebian, M., Armitage, S. & Stokes, S., 2006. Holocene slip-rate on the Sabzevar thrust fault, NE Iran, determined using optically-stimulated luminescence (OSL). *Earth planet. Sci. Lett.,* **245,** 673–684.

Fattahi, M., Walker, R., Khatib, M.M., Dolati, A. & Bahroudi, J., 2007. Slip-rate estimates and past earthquakes on the Doruneh fault, eastern Iran, *Geophys. J. Int.,* **168,** 691–709.

Hetzel, R., Niedermann, S., Tao, M., Kubik, P.W. & Strecker, M.R., 2006. Climatic versus tectonic control on river incision at the margin of NE Tibet: 10Be exposure dating of river terraces at the mountain front of the Qilian Shan, *J. geophys. Res.,* **111,** F03012.

Marsh, R.E., Prestwich, W.V., Rink, W.J. & Brennan, B.J., 2002. Monte Carlo determinations of the beta dose rate to tooth enamel, *Radiat. Measur.,* **35,** 609–616.

Masson, F., Anvari, M., Djamour, Y., Walpersdorf, A., Tavakoli, F., Daignières, M., Nankali, H. & Van Gorp, S., 2007. Large-scale velocity field and strain tensor in Iran inferred from GPS measurements: new insight for the present-day deformation pattern within NE Iran, *Geophys. J. Int.,* **170**(1), 436–440. doi:10.1111/j.1365-246X.2007.03477.x

Meyer, B. & Le Dortz, K., 2007. Strike-slip kinematics in Central and Eastern Iran: estimating fault slip-rates averaged over the Holocene, *Tectonics,* **26,** TC5009, doi:10.1029/2006TC002073.

Meyer, B., Mouthereau, F., Lacombe, O. & Agard, P., 2006. Evidence of Quaternary activity along the Deshir fault: implication for the Tertiary tectonics of Central Iran, *Geophys. J. Int.,* **164,** 192–201.

Murray, A.S. & Wintle, A.G., 2000. Luminescence dating of quartz using an improved single-aliquot regenerative-dose protocol, *Radiat. Measur.,* **32,** 57–73.

Nabavi, M.H., 1970. Geological Map of Yazd sheet (H9), scale 1:250,000, Geol. Surv. of Iran, Teheran.

Nishiizumi, K., Lal, D., Klein, J., Middleton, L. & Arnold, J.R., 1984. Production of ^{10}Be and ^{26}A1 by cosmic rays in terrestrial quartz and implications for erosion rates, *Nature,* **319,** 134–136.

Nishiizumi, K., Imamura, M., Caffee, M.W., Southonc, J.R., Finkel, R.C., & McAninch, J., 2007. Absolute calibration of 10Be AMS standards, *Nucl. Instrum. Methods Phys. Res., B Beam Interact. Mater. Atoms*, **258**(2), 403–413.

Oskin, M., Perg, L., Shelef, E., Strane, M., Gurney, E., Singer, B. & Zhang, X., 2008. Elevated shear-zone loading rate during an earthquake cluster in eastern California, *Geology,* **36**(6), 507–510, doi:10.1130/G24814A.1

Prescott, J.R. & Hutton, J.T., 1994. Cosmic ray contributions to dose rates for luminescence and ESR dating: large depths and long-term time variations, *Radiat. Measur.,* **23,** 497–500.

Regard, V. *et al*., 2006. 10 Be dating of alluvial deposits from Southeastern Iran (The Hormoz Strait area), *Palaeogeogr., Palaeoclimatol., Palaeoecol.,* **242,** 36–53.

Repka, J.L., Anderson, R.S. & Finkel, R.C., 1997. Cosmogenic dating of fluvial terraces, Fremont River, Utah, *Earth planet. Sci. Lett.,* **152,** 59–73.

Ritz, J.F., Brown, E.T., Bourlès, D.L., Philip, H., Schlupp, A., Raisbeck, G.M., Yiou, F. & Enkhtuvshin, B., 1995. Slip-rates along active faults estimated with cosmic-ray-exposure dates: application to the Bogd Fault, Gobi-Altaı¨, Mongolia, *Geology,* **23,** 1019–1022.

Soheili, M., 1981. Geological Map of Anar sheet (H10), scale 1:250,000, Geol. Surv. of Iran, Teheran.

Siame, L. *et al*., 1997. Cosmogenic dating ranging from 20 to 700 ka of a series of alluvial fan surfaces affected by the El Tigre fault, Argentina, *Geology,* **25,** 975–978.

Stone, J.O., 2000. Air pressure and cosmogenic isotope production, *J. geophys. Res.,* **105**(B10), 23 753–13 759.

Van Der Woerd, J. *et al*., 1998. Holocene left slip-rate determined by cosmogenic surface dating on the Xidatan segment of the Kunlun fault (Qinghai, China), *Geology,* **26,** 695–698.

Vernant, P.H. *et al*., 2004. Present-day crustal deformation and plate kinematics in the Middle East constrained by GPS measurements in Iran and Northern Oman, *Geophys. J. Int.,* **157,** 381–398.

Walker, R. & Jackson, J., 2004. Active tectonics and late Cenozoic strain distribution in central and eastern Iran, *Tectonics,* **23,** TC5010, doi:10.1029/2003TC001529.